JOURNAL OF SOLID STATE CHEMISTRY 51, 17–37 (1984)

Charge Transfer Effects in α-Picoline Intercalate of FeOCl by Mössbauer Spectroscopy

G. A. FATSEAS, P. PALVADEAU, AND J. P. VENIEN

Laboratoire de Chimie des Solides, L.A. 279, 2, rue de la Houssinière, 44072 Nantes Cedex, France

Received December 8, 1982; in revised form June 29, 1983

A Mössbauer study was carried out between 4.2 and 296 K on a powder sample of α-picoline intercalate of FeOCl: $FeOCl(C_6H_7N)_{0.25}$. The spectra in the paramagnetic region ($T > 64$ K) show charge transfer effects reflected, principally, in the presence of Fe^{2+} atoms (14% at 64 K), in a temperature-dependent population ratio Fe^{3+}/Fe^{2+}, and also, in the appearance of an Fe^{m+} site of intermediate valency ($2 < m < 3$). Also, changes are observed in the hyperfine parameters of the Fe^{3+} site as compared to the corresponding site of the FeOCl matrix. From relative intensities arguments, the results are explained in terms of electron delocalization on the basis of a thermally activated electron exchange between Fe^{2+} and picolinium. The shapes of the spectra in the magnetic states of both FeOCl and $FeOCl(\alpha\text{-pic})_{0.25}$, indicate the presence of magnetically inequivalent iron sites and electronic relaxation effects attributed to the layered structure of the compounds.

1. Introduction

Over the last few years Mössbauer spectroscopy has largely contributed to an understanding of the charge transfer mechanisms occurring when organic or organometallic molecules are intercalated in the interlayer spacing of trivalent iron oxychloride, FeOCl. The observed hyperfine parameters and their temperature dependence for both the paramagnetic and magnetic states point to remarkable differences between pure FeOCl and the intercalated $FeOCl(G)_n$ compounds. These differences reflect, principally, charge transfer effects between the guest molecule (G) and the host lattice. We discuss below the results of a Mössbauer study on a powder sample of α-picoline intercalate $FeOCl(\alpha\text{-pic})_{0.25}$ ((called here after FeOCl(pic)) in relation to the nonintercalated FeOCl, and in the light of known results on other FeOCl intercalation compounds.

2. Experimental Section

2.1. Sample Preparation and Structural Information

The intercalation of α-picoline (CH_3–C_5H_4N) in iron oxychloride FeOCl was obtained by reaction at 100°C in sealed tubes. The resulting chemical composition of 0.25 was determined by chemical analysis of C and N and corresponds to a stoichiometric compound, in agreement with previous results (*1, 2*). X-ray single crystal study has confirmed the expansion of the Van der Waals gap (b axis) and the shift of the FeOCl layers in the ac plane (Table I). The picoline symmetry axis, containing the nitrogen atom, is inclined with respect to the

0022-4596/84 $3.00

TABLE I

CRYSTALLOGRAPHIC DATA OF $FeOCl(\alpha\text{-pic})_{0.25}$ AT ROOM TEMPERATURE COMPARED WITH THOSE OF FeOCl

	a (Å)	b (Å)	c(Å)	Interlayer expansion (Å)	Space group
$FeOCl(pic)_{0.25}$	3.792	13.39 × 2 26.78	3.334	5,49	*Immm* or *I*222
FeOCl	3.781	7.893	3.293		*Pmnm*

Note. One can see the interlayer expansion of the lattice along the b-axis in FeOCl(pic).

layers at an angle of approximately 50° (*3, 4*). Because of the symmetry of the molecular environment, a number of equivalent orientations exist, and the molecule resonates between these positions at a rate which depends on temperature (*5*). FeOCl belongs to the *Pmnm* space group. After intercalation, new extinctions appear, corresponding to a centered group *Immm* or *I*222. All iron atoms are octahedrally coordinated by four oxygen and two chloride ions. On intercalation, the FeOCl sheets are separated, thus creating large cavities for the guest molecules. The Cl^- sheets in adjacent layers are above each other and generate a set of orthorhombic cells in the Van der Waals gap.

2.2. Fe^{57} Mössbauer Spectroscopy and Fitting of Results

The Mössbauer spectra were obtained with a constant-acceleration automatic-folding Elscint-type spectrometer using a room temperature $Co^{57}(Rh)$ source in a transmission geometry. The Mössbauer sample contained 10 mg natural iron per square centimeter and was studied in the temperature region $4.2 \leq T \leq 296$ K with an Oxford Instruments variable temperature cryostat (stability better than 0.1 K). The spectra were computed with a least squares routine using Lorentzian lines and able to fit Mössbauer spectra with any combination of quadrupole and Zeeman hyperfine interactions. The best fits are shown in Figs. 1 and 2 and are explained below.

2.2.1. Paramagnetic region ($T \gtrsim 64$ K). In the lower temperature range the spectra contain two quadrupole-split doublets, strong and weak, corresponding, respectively, to Fe^{3+} and Fe^{2+} atoms (Fig. 1). Above approximately 160 K, an additional quadrupole doublet is observed, hereafter called the Fe^{m+} doublet, with an intermediate isomer shift value and a low quadrupole splitting. The presence of this Fe^{m+} site is inferred from the central part of the spectra located in the velocity interval $0.3 \leq v \leq 0.5$ mm/sec, which exhibits stronger absorption than expected from the superposition of the Fe^{3+} and Fe^{2+} doublets alone; the intensity increases with increasing temperature above 165 K. Any attempt to fit the spectra without this site, by using either free parameters or alternative constraints on the line positions, or on the linewidth or on the intensity ratios of the remaining Fe^{3+} and Fe^{2+} sites failed; the best chi-squared values without the Fe^{m+} site are 5.0 at 296 K, 2.5 at 210 K, and 2.0 at 165 K. These values become, respectively, 2.6, 1.69, and 1.94 when the Fe^{m+} site is introduced.

It is appropriate to note that the spectra were fitted with large full linewidths at half maximum (FWHM), compared to the experimental linewidth of a thin metallic iron absorber (0.25 mm/sec). The values fell in the range 0.44 ± 0.02 mm/sec for Fe^{3+} (free parameter), from 0.30 to 0.35 mm/sec for Fe^{2+} in the whole paramagnetic region (free parameter), and 0.40 (fixed) for Fe^{m+}. Due to the absence of net resonance peak in the velocity region ofFe^{m+}, the site was fitted with fixed parameters, after several test with slightly different sets of δ, ΔE, and FWHM values. The asymetry of the Fe^{3+} doublet requires explanation: this doublet is slightly asymetric, with a nearly temperature-independent intensity ratio $R = I^+/I^-$ covering the range 1.07 ± 0.03 in the whole paramagnetic region. Thus, the inversion of

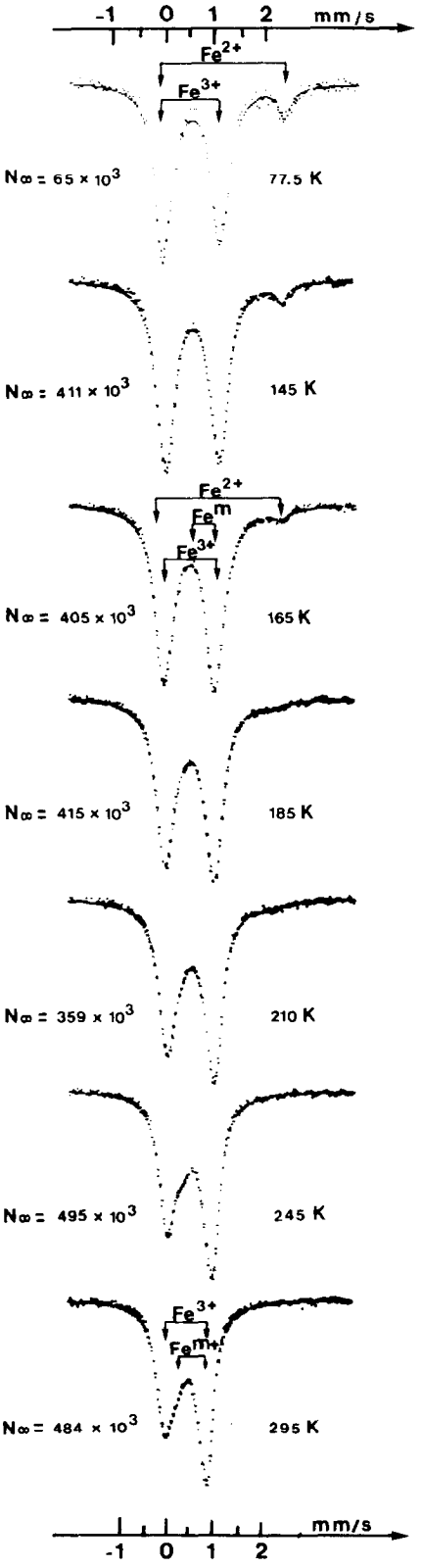

the intensity ratio of the strong peaks occurring around 155 K (Fig. 1) is phenomenological; it is only due to the progressive decrease in intensity of the Fe^{2+} doublet. Figures 3, 4, and 5 illustrate, respectively, the fitted hyperfine parameters: relative intensities (I), isomer shift (δ) (relative to the iron metal at 296 K), and the quadrupole splitting $\Delta E = \frac{1}{2}eV_{zz}Q\sqrt{1 + n^2/3}$ of each site in the whole paramagnetic region.

2.2.2. Magnetic region (4.2 ≤ T ≤ 64 K) (Fig. 2). With the exception of the spectrum at 64 K in which any existing weak magnetic hyperfine patterns were neglected, the spectra of this region were fitted either with pure Zeeman patterns, at $4.2 \leq T \leq 50$ K, or with a superposition of Zeeman patterns and paramagnetic doublets ($50 < T < 64$ K). In this last subregion (Fig. 2), proceeding from 64 K to lower temperatures, the Fe^{3+} paramagnetic doublet decreases in intensity and vanishes below approximately 50 K. Also the right-hand peak of the Fe^{2+} doublet is seen to vanish between roughly 55 and 57 K. These two doublets were fitted with δ and ΔE values for each respective temperature-dependence curve of the paramagnetic region (Figs. 4, 5). The Zeeman pattern contribution (the six broadened absorption peaks) was fitted by a discrete distribution of magnetic hyperfine fields (H), as illustrated by the normalized distribution probability function $P_T(H)$ for each temperature T (Fig. 6); each spectrum is a superposition of sextets which differs only in the value of H (fixed) and depths (to be fitted). The discrete H values are shown in the probability histogram (full line rectangles). $P(H)dH$ is the probability density function for H, i.e.,

FIG. 1. Fitted spectra of FeOCl(pic) in the paramagnetic state. The zero velocity is the centroid of the spectrum of the metallic iron at 296 K. All sites were fitted with broadened lines compared with the experimental linewidth of a thin iron metallic absorber (see Sect. 2.2.1).

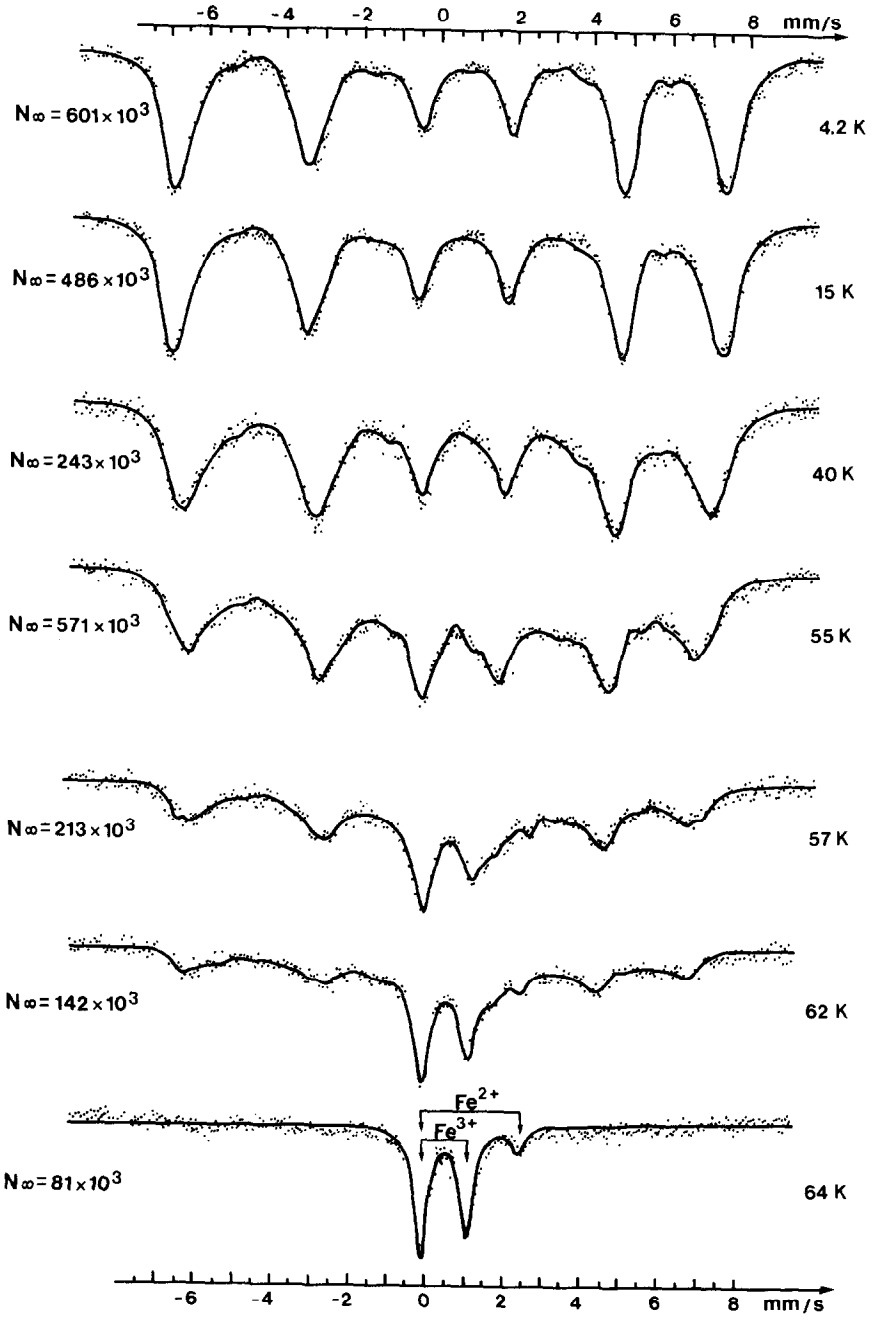

FIG. 2. Same caption as in Fig. 1 for the magnetic state. The full line represents the best least squares fit, obtained with a discrete hyperfine magnetic field values distribution. The spectra show evidence of relaxation effects (see text). Fitted FWHM = 0.60 mm/sec. The spectrum at 64 K represents mainly the paramagnetic state.

the ratio of iron sites having, at temperature T, hyperfine fields lying between H and $H + dH$ (*6, 7*). Some asymmetry is observed in the line intensities of the sextets reflected in a small deviation from the fitted 3:2:1 intensity ratios (see Sect. 3.5). The isomer

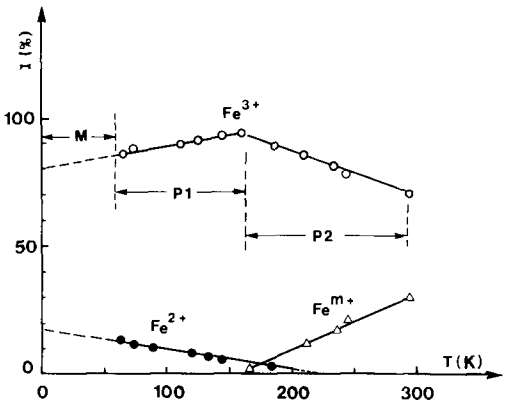

FIG. 3. Temperature dependence of the relative intensities (I) (fractional absorption areas) of Fe^{3+}, Fe^{2+}, and Fe^{m+} sites (I is equal to the fractional amount of iron for each site if all sites have identical f factors). Due to the unresolved Fe^{2+} Zeeman component in the spectra of the magnetic (M) region, the intensities are unknown in this region (see text). The weakness of the Fe^{2+} intensity above 210 K precludes any accurate determination of the temperature at which the Fe^{2+} site vanishes inside the 230 ± 10 K region (error for all points ±1%).

shift, the quadrupole splitting (ε_m), and the linewidth were constrained to be constant for all sites and at all temperatures with the following values chosen after some preliminary fitting: $\delta = 0.49 \pm 0.01$ mm/sec, $\varepsilon_m =$

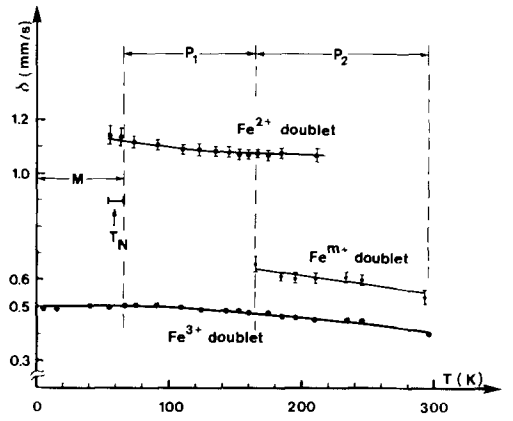

FIG. 4. Isomer (δ) versus temperature (relative to the metallic iron at 296 K) for the Fe^{3+}, Fe^{2+}, and Fe^{m+} sites. The unknown δ value in the magnetic (M) region is due to the unresolved Fe^{2+} Zeeman contribution in this region (bars and filled circles indicate errors).

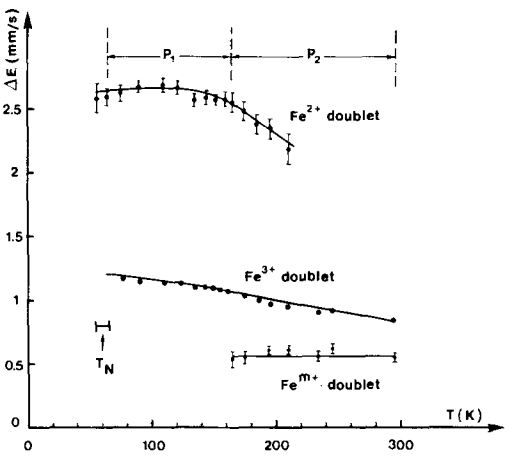

FIG. 5. Quadrupole hyperfine splitting (ΔE) in the paramagnetic state versus temperature, for the Fe^{3+}, Fe^{2+}, and Fe^{m+} sites. The quadrupole splitting in the magnetic state (ε_m) is equal to −0.50 mm/sec for all sites (see Sect. 2.2.2) (bars and filled circles indicate errors).

−0.50 mm/sec, and FWHM = 0.60 mm/sec, (where $\varepsilon_m = 1/2[|v_6 - v_5| - |v_2 - v_1|]$ and v_i is the velocity in millimeters per second of the ith line of the sextet). The preliminary fitting enabled us, also, to conclude that the solution with Zeeman patterns ($\Theta = 0$, $\eta = 0$) is a good approximation; other solutions with a discrete distribution of Θ values (Θ: angle between H and V_{zz}) and a unique H value were not satisfactory as judged by the poor chi-squared values.

The "identification problem" of specifying the relative contributions of the Fe^{3+} and Fe^{2+} atoms to the whole spectrum at a given temperature was not resolved; according to the fitted value of 0.49 mm/sec for δ, the sites reflect the existence of Fe^{3+} ions. This is a reasonable conclusion for sites associated with H values higher than about 300 kOe which, according to H value systematics for iron compounds, are too high to be attributed to Fe^{2+} ions (known H_{max}: 344 kOe for FeF_2). This is not, however, the case for the lower H values which can belong to both Fe^{3+} and Fe^{2+} (in which case the Fe^{2+} sextets would be fitted with

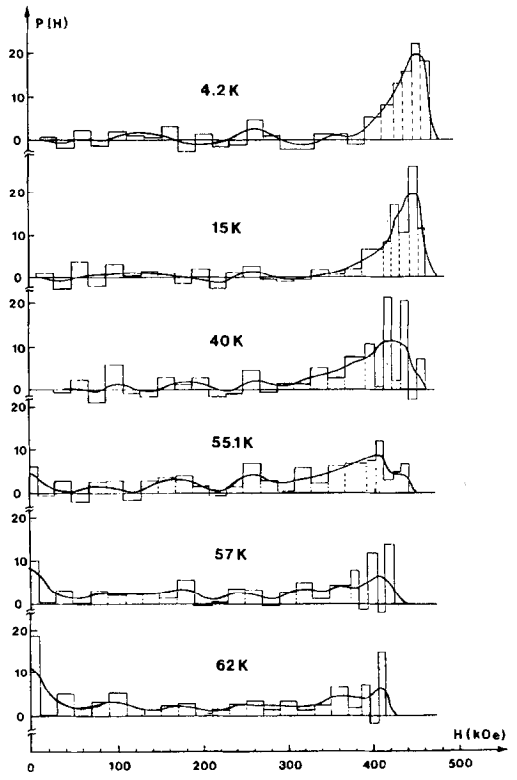

FIG. 6. Temperature dependence of the normalized distribution probability function $P_T(H)$ for the set of discrete hyperfine magnetic field values (H) of Fig. 2. The discrete H values are shown in the probability histograms (full-line rectangles).

an isomer shift close to 1 mm/sec). Unfortunately, the Fe^{2+} sextets are smeared out by crystalline fields and hidden inside the stronger Fe^{3+} sextets, in a manner similar to previously reported results (*7–9*). They are manifested, visually, by only one peak located at 5.9 mm/sec, outside the absorption region (Fig. 2). This precludes the determination of the Fe^{2+} contribution. We can, however, give an order of magnitude of H and ε_m which could fit the above peak considered as the sixth peak of a Fe^{2+} sextet, if we adopt a reasonable isomer shift of 1.20 mm/sec, taken from the extrapolation of the $\delta(T)$ curve of Fig. 4; some good sets of values are (H = 290 kOe, ε_m = −0.2), (H = 280 kOe, ε_m = 0.2 mm/sec), (H = 260 kOe, ε_m = 0.5 mm/sec), and (H = 230 kOe, ε_m = 1.4 mm/sec).

3. Discussion

3.1. Charge Transfer Effects

Different aspects of the charge transfer effects can be discussed via the isomer shift, the quadrupole interaction, and the relative intensities of the different sites in the paramagnetic region.

We discuss, first, the relative intensities (I) given in Fig. 3, as obtained from the fitted fractional absorption areas of the respective iron sites. These values are considered to be equal to the relative iron concentrations, which implies the assumption of an identical recoil free fraction (f) for all three paramagnetic sites. This assumption is usually adopted in the Mössbauer studies of "multisite" iron compounds (*10–12*) because of the difficulty of obtaining an unambiguous evaluation of the f parameter for each site (viz., thickness corrections, nonlinearity of the temperature dependent absorption-area curves, difficulties in the evaluation of the contribution of the second order Doppler effect on the δ (T) curve). The assumption is not, however, unreasonable in our case, as indicated in the next paragraph.

With this assumption in mind, we discuss the relative intensities of Fig. 3 as follows: at the onset of the paramagnetic region, the simultaneous presence of Fe^{3+} and Fe^{2+} atoms shows that electrons are donated by the intercalated picoline and that they are "trapped" by part of the host Fe^{3+} atoms. At 64 K, the results can be modeled if about 14% Fe^{3+} are assumed to be electron acceptors and become Fe^{2+} atoms via the charge transfer reaction

$$Fe^{3+} + \text{picoline} \rightarrow Fe^{2+} + \text{picoline}^+$$

where picoline$^+$ represents the picolinium ion.

It is evident, from the temperature-dependent intensities observed at $T > 64$ K (and holding also, probably at lower temperature), that this charge transfer reaction must be understood as a dynamic electron fluctuation written as

$$Fe^{3+} + \text{picoline} \rightleftarrows Fe^{2+} + \text{picolinium}.$$

In this case, the temperature-dependent intensity can be explained by a slow electron exchange between Fe^{2+} and picolinium with a mean life time (t) longer than the nuclear precession time τ ($t > \tau$, $\tau \simeq 10^{-7}$ sec). Under this condition, the Fe^{2+} and Fe^{3+} states are observed as distinct sites. The fact that the Fe^{2+} intensity decreases when T increases (reaching 5% Fe^{2+} at 160 K, with 95% Fe^{3+}), shows that a progressively greater number of Fe^{2+} ions are involved in the transfer process, which implies the existence of inequivalent Fe^{2+}–picolinium pairs that are thermally activated at different temperatures. This inequivalence is in accord with the broadened fitted lines of the paramagnetic spectra and can result from inequivalent environments of the Fe^{2+} atoms, due to different orientations of the picoline molecule (*5*) and/or to the existing different Fe–Fe distances.

In the framework of this electron-exchange mechanism we can also explain the presence of the Fe^{m+} site of intermediate valency ($2 < m < 3$) in the P_2 region ($160 < T \leq 296$ K): we assume that the transfer process rate increases with T and, above about 155 K, reaches the condition $t \leq \tau$ which renders the Fe^{2+} and Fe^{3+} atoms indistinguishable; only an Fe^{m+} site is detectable. The simultaneous presence of the Fe^{m+}, Fe^{2+}, and Fe^{3+} sites between 160 and 230 K shows that the fast transfer process occurs only for part of the inequivalent Fe^{2+}–picolinium pairs at a given temperature, and that greater numbers of Fe^{2+} atoms reach this condition when T increases. This causes the Fe^{m+} intensity to increase, reaching 29% at 296 K at the expense of both the Fe^{2+} and the Fe^{3+} intensities. These decrease, the first from 5% at 160 K to 0 at 230 ± 10 K, and the second, from 95% at 160 K to 71% at 296 K. The further decrease of the Fe^{3+} intensity above 230 K, in the absence of Fe^{2+} atoms, is more difficult to explain. It could be that some of the Fe^{3+} atoms of the host are involved in the fast transfer process. Such a mechanism, although complex, can be anticipated from magnetic nuclear resonance measurements which have shown that the picoline molecules move throughout the lattice above 240 K (*5*), in a manner similar to the isostructural $VOCl(pic)_{0.25}$ (*3*). If the molecule moves during the time that the electron resides thereon, it could exchange electrons with some neighboring Fe^{3+} ions. This would result in the observed increase of the Fe^{m+} intensity and the decrease of Fe^{3+} above ≃240 K.

3.2. Application of the Lotgering and Van Diepen Model

The correlation of the charge transfer process with the existence of inequivalent Fe^{2+}–picolinium pairs proposed here, can be further discussed in the light of the results as reported by Lotgering and Van Diepen (*13*) and by Grandjean and Gerard (*14*) on mixed ferrites. In these two studies, the observed charge transfer effects, although described by different mechanisms (hopping between Fe^{3+}–Fe^{2+} octahedral pairs in Ref. (*13*), or hopping through a conduction band in Ref. (*14*)) were related to inequivalent octahedral Fe^{3+} and Fe^{2+} sites, due to inequivalent environments arising from the random distribution of the different cations. This inequivalence was represented by Lotgering et Van Diepen (*13*) by a potential difference U_0 between the Fe^{3+} atoms and the exchange electron, which quantity varies from atom to atom, and by a potential barrier representing the "self-trapping" energy from local lattice

deformation and electrical polarization. In this model of "double potential well," both the thermal fraction of iron atoms participating in the exchange process, i.e., the fraction of atoms for which the electron has sufficient energy ($U_0 + q$) to pass the barrier, and the electron exchange frequency ν_{hop} of this fraction, are determined by a Boltzmann distribution (formulae 1,3 in Ref. (*13*)). Applying this model to our inequivalent Fe^{2+}–picolinium pairs and using the same notation as in Ref. (*13*) for the velocity region in which the Fe^{m+} site is observed, we find $v_2 - v_1 = 1.12$ mm/sec at 165 K (difference between the two lines of the Fe^{3+} doublet (Fig. 1). This value corresponds to a critical electron exchange frequency ν_{cr} equal to 8.14×10^{-7} sec^{-1} through the indetermination principle (1 mm/sec = 4.8×10^{-8} eV) and lead to a self trapping energy $q = 0.024$ eV and to a U_0 value of several millielectron volts. This very small value of U_0 indicates a very small variation in U_0 over the various sites (existence of very slightly inequivalent iron sites) and is compatible with the fitted large linewidth. It is interesting to note that although the q value represents only an order of magnitude estimate, it is very close to the "activation energy" that one calculates from the Fe^{m+} relative-intensity curve of Fig. 3, assuming a thermal activation process $I = I_0 e^{-E/kT}$ for this intensity (I). Taking $I_0 = 2\%$ at 165 K, one can draw, for some values of I, the curve $\log I/I_0$ versus $1/T$ and calculate, from the slope (E/k), the activation energy E. This gives an "average" value equal to 0.045 eV, the curve $\log I/I_0$ ($1/T$) deviating slightly from linearity.

The Lotgering and Van Diepen model can explain our results as follows: for $T <$ 165 K, the electron exchange frequency ν_{hop} increases when T increases, but it remains lower than ν_{cr} in the whole P_1 region. The Fe^{2+} and Fe^{3+} peaks are well separated, and the Fe^{2+} intensity decreases when T increases, as Fe^{2+} atoms with increasingly higher U_0 became involved in this slow-rate process. At temperatures $T > 165$ K, the temperature-dependent ν_{hop} reaches the condition $\nu_{hop} \gtrsim \nu_{cr}$ which produces the Fe^{m+} site whose concentration increases with T, as more and more Fe^{2+} corresponding to higher U_0 reach the condition of fast-rate exchange process.

Herber and Cassel (*15*), who observed both Fe^{3+} and Fe^{2+} sites in FeOCl(krypt-22), explained the decrease of Fe^{2+} with increasing temperature and its disappearance above $\simeq$140 K, from the weakness of the chemical interaction between the guest and the Fe^{2+} atoms via a mechanism analogous to that reported by Drickamer (*16*). The decreasing temperature in the Herber and Cassel experiment is qualitatively equivalent to the increasing pressure of Drickamer's investigation; according to Drickamer, the reduction $Fe^{3+} \rightarrow Fe^{2+}$ is, in fact, an exothermic process involving the transfer of an electron from the ligands to the iron, due to changes in the electronic energy levels of the ferric ions.

This explanation implies that Fe^{3+} and Fe^{2+} contribute to the Mössbauer spectra in a manner similar to other cases such as spinel-type minerals (*17*) and several oxides (*18*). This involves the Drickamer model. This condition is not satisfied in our spectra in which, at $T > 160$ K, dynamic charge effects occur on the time scale of the Mössbauer effect.

3.3. Significance of the Relative Intensities (I) in the Case of Unequal f Factors for Fe^{3+} and Fe^{2+}

Here we present, first, two arguments based on stoichiometry consistent with the assumption of "identical" f factors for all sites and, next, a more quantitative evaluation of the Fe^{3+} and Fe^{2+} populations when the difference in f factors is taken into account.

The first argument concerns the Fe^{2+} in-

tensity maximum at low temperature. According to the chemical formula FeOCl $(pic)_{0.25}$, the transfer of all the mobile guest electron implies the presence of 25% Fe^{2+} atoms at 4.2 K, if the transferred electrons are completely localized on Fe^{3+} atoms of the host. This value is approached by the extrapolation to low temperatures of the Fe^{2+} intensity curve ($I \simeq 20\%$) (Fig. 3), assuming that the observed temperature dependence of this curve above 64 K also holds at the low temperature region (one should recall that, due to the unresolved Fe^{2+} sextets, this intensity has not determined in the "magnetic" spectra).

The second argument concerns the "fast transfer process" at $T > 160$ K; in this temperature region, the Fe^{2+} intensity approaches zero at 230 ± 10 K and corresponds to the situation in which all the Fe^{2+} ions are involved in the fast transfer process, thus forming the Fe^{m+} site. The Fe^{m+} intensity must be a maximum at this temperature, and equal to 25%. Our data give about 20% with a further increase to 30% at 296 K (this last point having be already discussed in the text). The discrepancies could be due to an overestimate of the extrapolated Fe^{2+} intensity at 4.2 K, in which case some delocalization of the transfer electrons would exist even in low temperatures, or else, to possible small difference in the Mössbauer factor f between the Fe^{3+} and the Fe^{2+} atoms.

A quantitative evaluation of the Fe^{3+} and Fe^{2+} populations from difference in f factors for these two sites can be carried out by exploiting to the temperature region $T > 78$ K, the $\delta(T)$ curves of Fig. 4 and the absorption areas $\ln[A(T)/A(78)]$ of each site illustrated in Fig. 7. The respective slopes of these two curves for Fe^{3+}, in their linear regions, are

$$\frac{d(\delta)}{dT} = (-4.60 \pm 0.20) \times 10^{-4} \text{ mm sec}^{-1} \text{ K}^{-1} \quad (160 \lesssim T \lesssim 296 \text{ K})$$

$$\frac{d \ln\left[\frac{A(T)}{A(78)}\right]}{dT} = (-4.10 \pm 0.20) \times 10^{-3} \text{ K}^{-1} \quad (185 \lesssim T \lesssim 296 \text{ K}).$$

These values can be used to estimate an effective vibrating mass M_{eff} (Fe^{3+}) for the Fe^{57} nucleus and a "Debye" temperature $\theta_{M'}$ (Fe^{3+}) from the two known formulae (see Refs. (*19–21*))

$$M_{\text{eff}} = 4.1684 \times 10^{-2} \left(\frac{d\delta}{dT}\right)^{-1}$$

and

$$\theta_{M'} = 4.3202 \times 10^2 \left(\frac{d\delta}{dT}\right)^{1/2} \left[\left(\frac{d \ln\left(\frac{A(T)}{A(78)}\right)}{dT}\right)\right]^{-1/2}$$

This yields $\Theta_{M'}(Fe^{3+}) = 145$ K and $M_{\text{eff}} = 91$ amu, in good agreement with the values

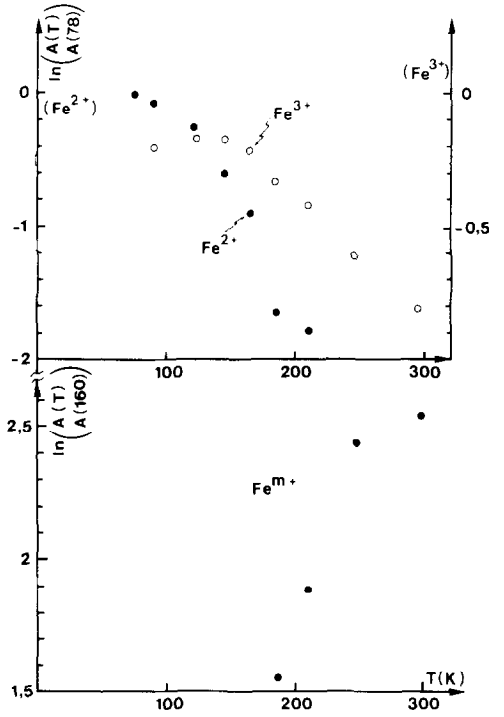

FIG. 7. Temperature dependence of the absorption area (A) relative to the area at 78 K for Fe^{2+} and Fe^{3+} and relative to 160 K for Fe^{m+}.

given by Herber *et al.* for other intercalated FeOCl compounds (*15, 19*). Using these two values and supposing that $\Theta_{M'}$ can be considered as a Debye temperature (Θ_D), which is a very tentative assumption (see, for example, Refs. (*11, 22*)), we can calculate the f factor at various temperatures from the formula (Debye model in the high temperature approximation $T > \Theta_D/2$)

$$f(Fe^{3+}) = \exp - \left[\frac{3}{2}\frac{E_R}{k\Theta_D} + \frac{6E_R T}{k\Theta_D^2}\right]$$

where E_R (eV) $= (5.37 \times 10^{-4} E_0^2$ (keV))$/M$ (amu). This yields the $f(T)$ curve for Fe^{3+} (Fig. 8) which is linear in the temperature region of the Figure ($f = 0.64$ at 78 K, $f = 0.47$ at 160 K (temperature region in which only Fe^{3+} and Fe^{2+} exist)).

The same calculation for Fe^{2+} is less accurate because of the difficulty of evaluating the slopes of $\delta(T)$ and $A(T)$ (nonlinearity for $A(T)$, low precision for $\delta(T)$ due to the low intensity of the Fe^{2+} site spectrum). We can, however, take a reasonable mean slope $d(\delta)/dT$ equal to -1.50×10^{-4} mm sec^{-1} K^{-1} ($150 \lesssim T \lesssim 210$ K) (Fig. 4) and calculate, similar to the case of Fe^{3+}, $f(T)$ curves for various values of $\theta_{M'}$. In this manner, we have obtained the $f(T)$ curves

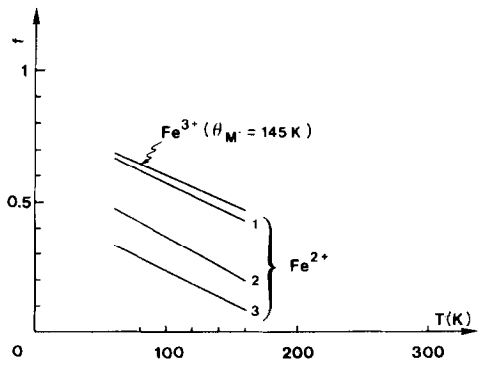

FIG. 8. Temperature dependence of the Mössbauer f factors for Fe^{3+} and Fe^{2+}. For Fe^{3+}, f was calculated, at a given temperature, from $\theta_{M'} = 145$ K (see text). For Fe^{2+}, three $f(T)$ curves were calculated, corresponding to $\theta_{M'} = 76$ K (curve 1), 54 K (curve 2), and 44 K (curve 3).

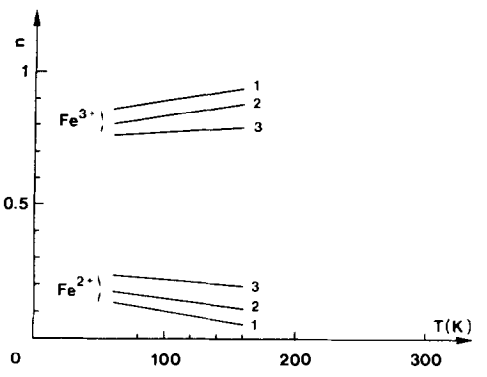

FIG. 9. Temperature dependence of the fractional amount of iron (n) of the Fe^{3+} and Fe^{2+} populations calculated at a given temperature from the corresponding I values of Fig. 4 and the f values of Fig. 8 (see text). Three pairs of curves are indicated: pair 1 calculated from the f factors $f(Fe^{3+})$ and $f(Fe^{2+})$ no. 1 of Fig. 8, pair 2 from $f(Fe^{3+})$ and $f(Fe^{2+})$ no. 2, and pair 3 from $f(Fe^{3+})$ and $f(Fe^{2+})$ no. 3.

corresponding to $\theta_{M'}(Fe^{2+}) = 76$, 54, and 44 K (Fig. 8). The whole of Fig. 8 can now be used to evaluate the fractional amount (n) of Fe^{3+} and Fe^{2+} at various temperatures, from the corresponding intensities (I) of Fig. 3. For the thin absorber approximation we have applied the formula

$$\frac{n^{3+}}{n^{2+}} = \frac{I^{3+}}{I^{2+}} \times \frac{f^{2+}}{f^{3+}}$$

which leads to the results of Fig. 9. Three pairs of (Fe^{3+}, Fe^{2+}) curves are indicated in this figure: pair was calculated from $f(Fe^{3+})$ and $f(Fe^{2+})$ no. 1 of Fig. 8 ($\Theta_{M'}(Fe^{3+}) = 145$ K, $\theta_{M'}(Fe^{2+}) = 76$ K), pair 2 from $f(Fe^{3+})$ and $f(Fe^{2+})$ no. 2 ($\theta_{M'}(Fe^{2+}) = 54$ K) and pair 3 from $f(Fe^{3+})$ and $f(Fe^{2+})$ no. 3 ($\theta_{M'}(Fe^{2+}) = 44$ K). One can see in Fig. 8 that, for $\Theta_{M'} = 76$ K, the f values for Fe^{3+} and for Fe^{2+} (curve 1) are very close, which leads to practically identical $n(T)$ and $I(T)$ curves for Fe^{3+} and Fe^{2+} (compare $I^{3+}(T)$ and $I^{2+}(T)$, Fig. 4, with the respective $n^{3+}(T)$ and $n^{2+}(T)$ (pair 1) of Fig. 9). Thus, if $\Theta_{M'}(Fe^{2+}) \simeq 76$ K, our assumption, in which the fractional areas (I) reflect the fractional amount of iron, is valid (see Sect.

3.1), and the disappearance of the Fe^{2+} doublet close to 230 K is due to the vanishing of the Fe^{2+} population. We note that the value of 76 K for $\Theta_{M'}(Fe^{2+})$ is reasonable when compared to $\Theta_{M'} = 60$ K, reported for Fe OCl(krypt) (*15*). Furthermore, it is not restrictive; any lower value in the approximate range $65 \lesssim \Theta_{M'} \lesssim 77$, reinforces our model, because it leads to slightly higher n values for Fe^{2+} compared with those given by the n^{2+} curve 1. It is thus closer to the value predicted by the stoichiometry arguments advanced at the beginning of the present section (closer to 25% Fe^{2+} at 4.2 K, and nonzero Fe^{2+} at 230 K, which is more consistent with the 20% Fe^{m+} at this temperature). We exclude all $\Theta_{M'}(Fe^{2+})$ values above about 77 K because they lead to $f(Fe^{2+}) > f(Fe^{3+})$ and, thus, to an unreasonably small concentration of Fe^{2+} ions. We exclude, also, all values below about 44 K because they lead to Fe^{2+} populations which are too high and practically temperature independent and even (for $\Theta_{M'} \lesssim 41$ K) to a positive temperature variation. This is inconsistent with the experimentally detected Fe^{m+} site concentration at $T \geq 165$ K and with other results in which the Fe^{2+} involved in various charge transfer processes decreases with decreasing temperature (*15–17, 23*).

3.4. Isomer Shifts (δ) and Quadrupole Splitting (ΔE) of the Different Sites

3.4.1 Fe^{3+} site. This site has a δ value equal to 0.42 ± 0.01 mm/sec, at room temperature, lying within the range of 0.37 to 0.44 mm/sec for known Fe^{3+} oxides in octahedral environment and close to that of FeF_3 (0.45 mm/sec) (*24*). It is thus indicative of a Fe^{3+} ion. We must bear in mind, however, that in trivalent iron oxides, charge transfer to the vacant 3*d* and/or 4*s* orbitals from the filled O^{2-}–2p orbitals may generally occur (*25*).

To compare this site with the corresponding Fe^{3+} site of FeOCl, under the same experimental conditions, we have obtained the spectrum of Fig. 10. The comparison (Table II) shows that Fe^{3+} in FeOCl (pic) has both a higher δ and a lower ΔE value. Let us note that our δ and ΔE values for FeOCl are in agreement with values previously reported in six different publications covering the regions 0.395 ± 0.005 and 0.918 ± 0.012 mm/sec, respectively (*1, 2, 19, 21, 26, 27*). The higher δ for FeOCl (pic), as compared to that of FeOCl, is a seemingly general trend for the intercalated $FeOCl(G)_n$ compounds: values were reported in the range from 0.370 to 0.465 mm/

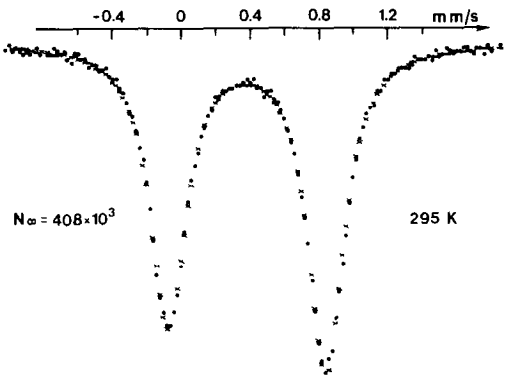

FIG. 10. Fitted spectrum of unintercalated FeOCl at 296 K (δ = 0.39, ΔE = 0.92, FWHM = 0.25 mm/sec). Note the narrow linewidth compared to that of FeO Cl(pic) and the absence of any absorption in the velocity region between the two lines.

TABLE II

COMPARISON OF THE HYPERFINE PARAMETERS OF THE Fe^{3+} SITE BETWEEN FeOCl(pic) AND FeOCl AT ROOM TEMPERATURE

Compound	δ (mm/sec)	ΔE (mm/sec)	FWHM (mm/sec)
$FeOCl(pic)_{0.25}$	0.42	0.82	0.44
FeOCl	0.39	0.92	0.25

Note. δ: Isomer shift relative to the iron metal at 296 K; ΔE: quadrupole splitting FWHM: full width at half maximum; error ± 0.01 mm/sec.

sec for the pyridine derivatives (*1, 2, 19*) and from 0.46 to 0.47 for the organometallic guests (ferrocene and cobaltocene) (*8, 27*). This trend was explained as reflecting a higher $3d$ density in the intercalated compounds which arises from electron transfer from the guest molecules (*2, 27*). This explanation is in agreement with the known correlation, for Fe^{57}, between δ and the number of $3d$ localized electrons, but may conceal, in light of results of Sawatzky and Van Der Woude (*25*), a more complex situation resulting from changes in both $3d$ and $4s$ configurations and delocalization (simple covalency), and from changes of the ns-core electrons wave functions by the ligand electrons (central covalency). The lower ΔE at room temperature, as compared to that of FeOCl, also obeys the rather general tendency: the reported values for FeOCl$(G)_n$ cover the region from 0.59 to 0.935 mm/sec (*1, 2, 19, 20, 27–29*), the smallest value being reported for $FeOCl(O_2C_2H_4)_{1/4}$ (*29*). Charge transfer effects and overlap distorsions which change with the nature and stoichiometry of the guests must be the origin of the observed discrepancies.

The isomer shift is temperature dependent above approximately 140 K with a negative slope $d\delta/dT = (-4.60 \pm 0.20) \times 10^{-4}$ mm sec^{-1} K^{-1} (Fig. 4). This value is lower than that expected from a "bare" atom in the high temperature limit (-7.305×10^{-4}) and much lower than the value reported for FeOCl (-6.18×10^{-4} at $78 \leq T \leq 300$ (*21*), -4.82 (*1*), and -5.29 (*19*). From values reported in the literature for two categories of FeOCl$(G)_n$ in which G is either a nitrogen containing molecule (pyridine or pyridine derivatives (*1, 2, 19, 20, 28*)) or organometallic molecule (ferrocene, cobaltocene (*8, 27*)), one notes that the smaller $d\delta/dT$ slope, as compared to FeOCl, represents a rather general trend; it indicates a higher effective mass (assuming that it results from the second order Doppler effect). This was explained as showing a stiffening of the lattice in FeOCl$(G)_n$, due to the replacement of the Van der Waals forces by ionic forces, resulting from the transferred electron (*1, 27*). Some exceptions involving greater slopes were, however, reported for $FeOCl(TEP)_{1/6}$, $FeOCl(TMP)_{1/6}$ (*20*), and FeOCl(dodecylamine)$_{1/4}$ (*19*).

In the paramagnetic region below $\simeq 140$ K, the isomer shift is nearly temperature independent. Herber and Maeda (*20*) have explained an analogous result of decreasing slope in the same region, in $FeOCl(TEP)_{1/6}$ and $FeOCl(TMP)_{1/6}$ (compared to the slope at higher temperature), in terms of the motional degree of freedom of the intercalated molecule. They argued that, in the low temperature region, the compound can be considered as a three-dimensional solid, because the interaction between the intercalated molecule and the atoms is large when compared to the mean of the thermal excitation energy kT.

The quadrupole splitting (ΔE) is temperature dependent, equal to 0.82 ± 0.01 mm/sec at 296 K and 1.17 ± 0.02 mm/sec at 77 K (Fig. 5). This contrasts with the reported essentially temperature-independent ΔE for FeOCl (*1, 21, 30*). This last temperature independence was explained by a thermal expansion of the lattice, resulting, principally, in an increase in the interlayer spacing and leaving the local environment of the Fe^{3+} atom unaffected (*21*). In the case of FeOCl(pic), the temperature dependent ΔE could be due to an anisotropic thermal expansion leading to a higher symmetry at higher temperatures for Fe^{3+}. Alternatively, it could arise from changes in charge transfer effects and overlap distortion due to a temperature-dependent bond strength between the iron and the picoline. It is known that in Fe^{3+} oxides the electric field gradient is very sensitive to the amount of overlap distortion of the closed shell Fe^{3+} orbitals by ligand orbitals and the amount of change transfer from ligand to empty Fe^{3+}

orbitals (*25*). Temperature-dependent ΔE values in the paramagnetic region were also observed for other intercalated FeOCl$(G)_n$ compounds (*1, 20*).

The intensity asymmetry of the Fe^{3+} quadrupole doublet observed in FeOCl (pic), is a well-established result for powder samples in both intercalated FeOCl (*20, 27*) and pure FeOCl (*1, 2, 21, 31*). Its origin was studied by Herber and Maeda (*20, 21*) who concluded, from the temperature independence of the intensity ratio $R = I^+/I^-$, that this asymetry is due to a preferential sample orientation, arising from the layered structure which places the *b* axis nearly perpendicular to the plane of the platelet. In the frame of this interpretation, the observed asymetry ratios $R = I^+/I^- = 1.05$ for FeOCl(pic) (Fig. 1) and $R = 1.10$ for the pure FeOCl (Fig. 7) at 296 K, show that both powdered compounds behave as oriented speicmens. Thus the V_{zz} axis has a conical distribution with a half angle of about 54° from the γ-ray direction. (The R ratio being very close to unity, the nonidentity of the I_π and I_σ components of the doublet is not important for an approximate value of this angle.)

The preferential orientation for a powder sample, is, of course, a texture effect and relates to the conical distribution of V_{zz}, one of assumptions made in the theory of the "magic angle" concept as applied to the texture problem (*32, 33*). To check these points, we tried to overcome the texture by two methods: first, we mixed the powder absorber with some boron nitride powder. No significant R-ratio change was observed. Second, we tried to apply the "magic angle" condition (*32*) by placing the absorber in a cryostat, and studied the angular dependence of the line intensities at room temperature by turning the sample around the vertical axis of the sample holder. The observed spectra showed some decrease in asymetry near the "magic angle" (54.7°), but the experimental conditions of this experiment preclude any unambiguous interpretation (small statistic, thickness effect).

3.4.2. Fe^{2+} site. This site is characterized by a typical isomer shift ($\delta = 1.07$ mm/sec at 210 K, 1.12 at 77 K) (Fig. 4) lying in the region anticipated for high spin Fe^{2+} in octahedrally coordinated iron oxides (*34, 35*). This is also supported by the high ΔE in the low temperature region (P_1) ($\Delta E = 2.62$ mm/sec at 77 K) (Fig. 5), together with the strong negative temperature dependence of ΔE at higher temperatures (2.56 mm/sec at 160 K, 2.18 mm/sec at 210 K). These two properties are indicative, within the crystal field theory, of Fe^{2+} ions with well-localized $3d$-β-spin electrons (*36*); they are compatible with the idea that the electrons donated by the picoline are "trapped" on Fe^{3+} atoms in the low temperature side of the paramagnetic P_1 region. Nevertheless, despite this localization, these iron atoms must be understood, according to a suggestion of Herber and Cassel for FeOCl(krypt-22) (*15*), as a dynamic equilibrium in the Fe^{3+}–picoline electronic exchange, and as existing on the time scale of the Mössbauer effect, rather than in the "infinite" time of any macroscopic measurement. The decreasing intensity of these atoms in the higher temperatures and the appearance of the Fe^{m+} site as a result of thermal activation process confirm this point of view. High-spin Fe^{2+} ions were also seen in other FeOCl$(g)_n$ compounds in previous Mössbauer studies: FeOCl$(VCp_2)_{1/6}$ and FeOCl$(MnCp_2)_{1/6}$ (*37*), FeOCl$(FeCp_2)_{1/6}$ (*8*), and FeOCl(krypt)$_{1/18}$ (*15*). It is interesting to note that the quadrupole splitting ΔE at 78 K is practically the same whether or not Fe^{2+} is involved in a charge transfer process at higher temperatures (present study: 2.62 mm/sec, and mixed ferrites: 2.66 mm/sec, Ref. (*13*). For some of the above compounds: 2.58 mm/sec, Refs. (8, 15)).

3.4.3. Fe^{m+} site. This site is associated with an isomer shift lying, over the whole

temperature region, between those of Fe^{3+} and Fe^{2+} atoms (0.54 mm/sec at 296 K, 0.65 at 165 K) (Fig. 4). One is tempted for this reason, and according to known results on isomer shift-mixed valency correlation for iron compounds (*24, 38*), to attribute to these atoms an intermediate valency, in the sense that m is not an ionic charge state but a lumped electronic state corresponding to an electronic density on the nucleus "intermediate" between those of Fe^{3+} and Fe^{2+}. This is also consistent with our model, in which the Fe^{m+} atoms arise in the fast electron exchange process between Fe^{2+} and picolinium. We try to give below some insight on the electronic state of this site by discussing the δ and δE values in light of the previous results.

In the previous numerous papers devoted to electron exchange between octahedral iron sites in spinel ferrites, there is, in fact, the interesting (but difficult) problem of finding a satisfactory description for a mixed iron-valency system involving the delocalization of the exchange electrons. In extreme cases the question arises whether exchange electrons are localized on two neighboring B sites or delocalized and extended over the entire octahedral sublattice (*39*). The most typical result of "localized" hopping is that of Lotgering and Van Diepen (*13*) on Zn^{2+} and Ti^{4+} mixed ferrites containing Fe^{3+} and Fe^{2+} ions, in which the iron site ($Fe^{exch.}$) from $Fe^{2+} \leftrightarrow Fe^{3+}$ electron exchange was attributed to isolated Fe^{3+}–Fe^{2+} pairs and was characterized by a weighted average of δ and ΔE values. This "localized" hopping was explained by the authors in terms of the inequivalence of the B sites arising from the Zn^{2+} and Ti^{4+} substitution which causes trapping of the electrons on favorable sites. On the other hand, stoichiometric magnetite (Fe_3O_4) is the most typical case of "delocalized" hopping. Although there is no agreement on the basic mechanisms in the numerous papers devoted to this compound (*40–42*), it seems to be established from Mössbauer spectroscopy (*39, 43, 44*) that the fast electron hopping above the Verwey temperature is a delocalized process consistent with certain properties appropriate to metallic conduction (*45*). This is also in agreement with estimates of the distance of neighboring B sites, which is close to the critical distance R_{cr} for the formation of a collective electron state (*46*). In the Mössbauer studies of Fe_3O_4 this "delocalized" hopping is reflected in a very small quadrupole splitting of both the "magnetic" and "paramagnetic" spectra (*39, 43, 47,* and references therein) which is considered to be a strong indication of delocalized hopping (*13*). A recent study on ferrous iron chalcogenides also showed the correlation between the minority spin $3d$ electron itineracy and the low quadrupole splitting (*36*). In our case, in which the Fe^{m+} site is due to the alternation of Fe^{2+} and Fe^{3+} sites in the fast $Fe^{2+} \leftrightarrow$ picolinium process, a weighted average value for δ and ΔE is given by (at any temperature $T < 210$ K in which Fe^{2+} exists) the mean value of those for the Fe^{3+} and Fe^{2+} sites. Taking δ, $\Delta E(Fe^{3+})$ and δ, $\Delta E(Fe^{2+})$ from Figs. 4 and 5, this yields, for δ, $\langle\delta\rangle = 0.765$ mm/sec (0.62) at 200 K and 0.780 mm/sec (0.65) at 160 K and, for ΔE, $\langle\Delta E\rangle = 1.64$ mm/sec (0.55) at 200 K and 1.80 mm/sec (0.55) at 160 K, (the corresponding experimental value for Fe^{m+} (Figs. 4, 5) given in parentheses for comparison with the calculated values). According to this analysis, the much smaller experimental ΔE, as compared to the weighted average value, could indicate some delocalization of the exchanged electrons. However, this "delocalization" must be limited within the Fe^{2+}–picolinium pairs in order to be consistent with our electronic transfer model.

For further information, it is instructive to use another criterion, the correlation between localized/delocalized $3d$ electrons and electrical conductivity in light of pre-

vious known results. According to those experiments, the existence of delocalized or localized electrons in an intercalated $FeOCl(G)_n$ compound implies that the electrical conductivity should increase (by a factor occasionally as high as 10^3) or should not change, respectively, in passing from FeOCl to $FeOCl(G)_n$ upon intercalation. The first case was encountered in $FeOCl[Fe(Cp_2)]_{0.16}$ (*8, 48*), $FeOCl(py)_{1/4}$, and $FeOCl(propyl)_{1/4}$ (*2*) and the second case in for $FeOCl[Fe(Cp)_2]_{0.16}$ (*27*). In light of this crude correlation and according to single crystal conductivity measurements (by the dc method) which show no significant differences between FeOCl(pic) and FeOCl in the temperature range $100\ K \leq T \leq 300\ K$ (*49*), one could argue either that there is no $3d$ delocalization in FeOCl(pic) or that the $3d$ delocalization implied in the Fe^{2+}–picolinium electron exchange does not influence the conductivity. This last explanation is based on the fact that the value of the activation energy deduced from the Fe^{m+} intensity curve (0.045 eV, see Sect. 3.2) is much lower than that deduced from the resistivity curve (0.33 eV, Ref. (*49*)). Other explanations could be suggested from the comparison of FeOCl(pic) with the compounds cited above. The comparison, for example, with $FeOCl[Fe(Cp)_2]_{0.16}$ shows that the number of iron atoms involved in the electron exchange could be an important parameter (all of the iron atoms in this last compound vs only 30% in FeOCl(pic) at room temperature).

3.5. Magnetic State

The spectra of this region, whose fitting was explained in Section 2.2.2, exhibit the following features.

A first feature is the very broad peaks of the spectrum at 4.2 K. Despite the large number of 25 discrete H values used for the fitting, the deduced line width is still very large (FWHM = 0.60 mm/sec).This large linewidth is a strong experimental indication of inequivalent iron sites. This is also reflected, as explained earlier, in the paramagnetic spectra (see Sect. 3.1). Here, however, the inequivalence can also result in multiple superexchange paths, via the oxygen atoms, which probably exist in this structure, in light of neutron diffraction results on pure FeOCl (*50*). The broadened spectra at low temperatures were also observed in several nitrogen-containing $FeOCl(G)_n$ compounds, indicative, according to the authors (*19*), of slightly inequivalent iron sites.

A second feature is the increasing broadening of the external lines, when the temperature rises from 4.2 to 64 K, and the growth of the inner lines at the expense of the outer lines (Fig. 2).

These results may be taken as typical features of electronic relaxation effects, which, in light of similar results on $FeOCl[Fe(Cp)_2]_{1/16}$ (*8*) and α-FeOOH (*51–53*), could be due to the layered structure of the compound. In this sense, the "static" fitting described in Section 2.2.2, with a simple superposition of independent Zeeman sextets and paramagnetic doublets above 57 K, and with a discrete set of Zeeman sextets at low temperatures, represents only a phenomenological approach. We know that in the case of the relaxation spectra, a Zeeman pattern may still exhibit broadened lines, even at low temperatures, if the electronic relaxation time is not very long compared to the lifetime of the excited nuclear state (*54*). Thus, our spectra could reflect relaxation behavior as well as sets of discrete H values contributed by magnetically inequivalent iron sites.

To obtain further experimental support, we have obtained the spectra of the pure FeOCl to determine whether or not its layered structure produces spectra reflecting the relaxation effects. The resulting spectra, which, to our knowledge, were never published (with the exception of the spec-

trum at 4.2 K), are illustrated in Fig. 11. Because of the much narrower lines at 4.2 K which reflects the simpler situation of a limited site number (only two sites were detected), the spectra of this figure could exhibit relaxation effects. This reinforces the idea that relaxation effects occur in FeOCl(pic), although the situation in this last compound seems to be more complex. In light of this comparison and of the similar results in the other layered materials cited above, one can tentatively assume that the layers, isolated by the interlayer spacing, present a superparamagnetic phenomenon of the type well known in thin films (*55, 56*) and in fine particles of iron and iron compounds (*57, 58*). Also supporting this idea of isolated layers is the reduction of the hyperfine field (≃456 kOe) as compared to the value of the high-spin ferric ion (≃620 kOe). This may reflect, apart from the covalent character of the compound (*59*), a zero-point spin reduction occurring in one or bidimensional magnetic systems (*60, 61*). A bidimensionality was proposed, in fact, for the unintercalated FeOCl as explanation for the reduced magnetic moment of 4.1 μ_b, as measured by neutron diffraction studies at 4.2 K (*50*). (A neutron diffraction measurement on FeOCl(pic) would be very instructive at this point.) It must be noted that the superparamagnetism proposed here does not necessarily apply to small particles or thin films. According to other reports, the effect can be observed even in a bulk material if it breaks up into magnetic clusters of a critical size so that superparamagnetic behavior may occur near the critical temperature (*52, 62–64*). This model implies the existence of collective spin flips within the clusters of various sizes, the clusters being due to lattice imperfections and/or impurities (*52, 65–67*), to statistical fluctuations in composition (*68–71*), or to the low magnetic dimensionality (*72–74*). In applying the above ideas to FeOCl(pic), we tentatively assume that the observed inequivalent iron sites reflect the existence of small clusters arising from some fundamental property such as a difference in strength of the superexchange linkage, the presence of iron chains of different lengths from lack of structural perfection, differences in in-

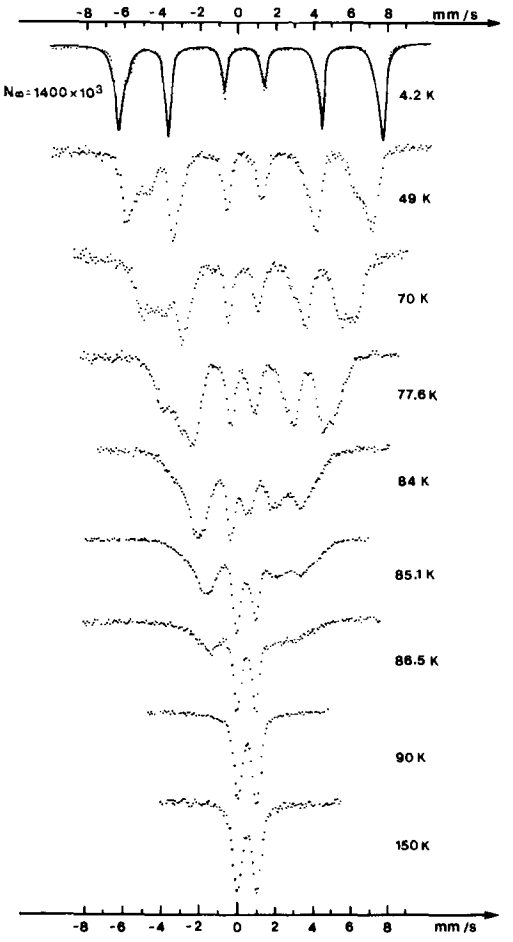

FIG. 11. Experimental spectra of FeOCl in the magnetic state ($T < 90$ K). The spectrum at 4.2 K was reasonably well fitted with a combined magnetic and quadrupole hyperfine interaction for two iron sites: (δ = 0.52 mm/sec, ε_m = −1.02 mm/sec, H = 434 kOe, n = 0.30, θ = 90°, relative intensity = 76%, FWHM = 0.32 mm/sec; and δ = 0.52 mm/sec, ε_m = −1.52 mm/sec, H = 406 kOe, n = 0.30, θ = 90°, relative intensity = 24%, FWHM = 0.48 mm/sec. The two iron sites are in agreement with the two magnetic sublattices reported earlier (*30, 50*). (The spectra at $T > 4.2$ K were not fitted).

teractions between the intercalated molecules and the atoms due to changes in the orientation of the molecules, from stacking faults or slippage of the layers, and/or charge (and spin) fluctuations related to the dynamics of the charge transfer effects. Although the above model (collective spin flips within the clusters) constitutes our favored explanation we cannot distinguish it unambiguously from the "motional narrowing" model. The latter involves unlikely individual spin fluctuations (although this last model is applied much more often to the paramagnetic substances). The difficulty of choosing between the two models is also present in α-FeOOH (compare Refs. (*52*) and (*53*)). We can, however, point out that the observed temporal effects on the time scale of the Mössbauer measurements make the existence of spatial distributions of hyperfine fields such as those observed in mixed oxides (*75*) and ferrites (*7*) much less probable.

The transition from the magnetic ordered to the paramagnetic state is not well defined because of the complex spectra near the transition. However, on the basis of the complete collapse of the Zeeman components, it can be deduced that the paramagnetic transition takes place close to 64 K (Fig. 2). This value is lower than that of FeOCl with $T_N = 91 \pm 1$ K, a result that seems to be the general trend for all the intercalation FeOCl compounds studied by Mössbauer spectroscopy: $T_N = 65$ K for $FeOCl(py)_{1/3}$ (*28*), ≃78 K for the pyridine derivatives $FeOCl(TEP)_{1/6}$ and $FeOCl(TMP)_{1/6}$ (*20*), and ≃75 K for FeOCl(ferrocene) (*8*). This comparison shows that the transferred electron from the guest, present in all the above compounds, decreases the stability of the antiferromagnetic structure in comparison with the unintercalated FeOCl. The contribution of the Fe^{2+} atoms which could be responsible for this decreasing magnetic stability in $FeOCl(py)_{1/4}$ FeOCl (ferrocene) and in the present study is not clear, because no Fe^{2+} ions were detected in $FeOCl(TEP)_{1/6}$ and $FeOCl(TMP)_{1/6}$.

Another general trend, worthy of note, is the higher hyperfine field (H) in the intercalated compounds, compared with that of FeOCl (430 kOe at 4.2 K); that is, $H = 456$ kOe in the present study, 448 in $FeOCl(pyr)_{1/3}$ (*28*), from 437 to 444 for several pyridine derivatives (*19*), 435 for FeOCl(ferrocene) (*8*), and nearly equal to that of FeOCl in $FeOCl(TEP)_{1/6}$ and $FeOCl(TMP)_{1/6}$ (*20*). The difference in zero point spin deviation (reflected in the contact Fermi term), in covalency (reflected to the contact term and to some orbital moment), and in the local symmetry (reflected in the dipolar contribution) may be the origin of this trend, but the relatively small difference between these values makes any quantitative interpretation difficult.

The direction of the hyperfine field at an Fe nucleus is determined by the exchange and dipole interactions between the electron spins and by the local crystalline field. If the latter dominates, the angle θ between V_{zz} and H is the same for all nuclei and the resulting magnetic structure of the material is such that the electron spins are more or less randomly oriented in space, but firmly fixed to a local symmetry axis. This produces a sharp six-line spectrum with a clearly defined value of θ. If, on the other hand, the anisotropy is weak, the exchange interactions impose the magnetic ordering irrespective of any local symmetry axis. In this latter case, the angle θ can vary widely, each angle corresponding to a different six-line spectrum. The reasonably good fitting with unique values of θ, $\theta = 0$ for FeOCl(pic) (see Sect. 2.2.2) and $\theta = 90°$ for the pure FeOCl (Refs. *30*, *31*, and present study) shows, first, that the magnetic properties of both compounds are governed, to a large degree, by crystalline anisotropy effects and second, as a reasonable approximation for an Fe^{3+} atom, that the easy di-

rection of magnetization lies within the layer plane in FeOCl(pic) (*ac* plane), in agreement with a single crystal Mössbauer study of $FeOCl(py)_{1/3}$ (*28*). The easy direction is perpendicular to the layer in pure FeOCl; this last result is deduced from $\theta = 90$, only in the light of a previous single crystal Mössbauer study which showed that the Fe^{3+} spins lie within the *bc* plane (*30*). This conclusion regarding pure FeOCl is consistent with a neutron diffraction study which indicated "cycloidal" magnetic order wherein the Fe^{3+} spins lie in the *bc* plane and rotate from one unit cell to the next along the *c* axis (*50*). This configuration implies a constant angle $\theta = 90°$. (In the above reasoning we considered that V_{zz} lies along the α axis within the layer, in both FeOCl and FeOCl(pic), according to prior results (*26, 28*)). The fixed direction for H along the V_{zz} axis in FeOCl(pic) would be reflected in the intensity of the second (and fifth) line of the Zeeman sextets making the intensity ratios $I_1 : I_2 : I_3$ equal to $3 : b : 1$ with $b = 4 \sin^2\beta/1^+ \cos^2\beta$ (β: angle between H and γ ray; I_i: the intensity of the lines of a sextet from negative to positive velocities). For $\beta = 54°$ between V_{zz} and γ ray deduced from the paramagnetic spectra, the asymetry would give rise to a very small deviation from the known 3 : 2 : 1 ratios toward 3 : 1.946 : 1. In fact, the experimental spectra at 4.2, 15, and 40 K (Fig. 2) show some small asymetry with a b value slightly higher than 2 (an angle of 56° would give $b = 2.10$), but the large number of sites and the constraints used in the fitting (see Sect. 2.2.2) make it difficult to obtain a more precise quantitative estimate.

The sign of the average value of the quadrupole interaction (ε_m) in the magnetic state was found to be negative as can be also seen from the relative separation of the 1,2 and 5,6 peaks of the experimental spectrum at 4.2 K, fitted with Zeeman components ($\theta = 0$, $\eta = 0$) (Fig. 2). The same sign can be deduced from the six-line spectra of FeO $Cl(py)_{1/3}$ (*19, 20, 28*) and $FeOCl(NH_3)_{3/4}$ (*20*), ($|v_6 - v_5| < |v_2 - v_1|$), but a positive sign can be deduced for $FeOCl(TEP)_{1/6}$ (*20*), $FeOCl(2\text{-pic})_{1/4}$ (*19*), $FeOCl(\text{butylamine})_{1/4}$ (*19*), and $FeOCl(\text{ferrocene})_{1/6}$ (*8*) from their six-line spectra, ($|v_6 - v_5| > |v_2 - v_1|$). Herber *et al.*, who discussed the relation between the sign of the quadrupole interaction (ε_m) and the structure and stoichiometry of the guest molecule in the FeOCl intercalation compounds, suggested a positive sign for $n < 1/4$ and a negative sign for $n > 1/3$ in the compound $FeOCl(G)_n$ (*19, 20*). Our result of a negative sign for ε_m in $FeOCl(pic)_{1/4}$ appears to be an exception to the above proposed rule and suggests that more tests are necessary (see Appendix). The sign of ε_m for FeOCl was found to be negative from the fitted spectrum at 4.2 K (Fig. 8): two iron sites with combined hyperfine magnetic and quadrupole interactions ($\theta = 90°$, $\eta = 0.30$, see caption, Fig. 11).

4. Conclusions

The intercalation of picoline in FeOCl is accompanied by a charge transfer of the nitrogen lone pair electrons of picoline to the FeOCl matrix. This charge transfer is reflected, principally, in the presence of the Fe^{2+} atoms on the low temperature side of the paramagnetic region and in changes of the hyperfine parameters of the Fe^{3+} site as compared to the corresponding Fe^{3+} site of the FeOCl matrix (higher δ, lower ΔE, larger linewidth, higher H, lower T_N). At higher temperatures, the charge transfer gives rise to a temperature-dependent population ratio Fe^{3+}/Fe^{2+} and to the appearance of an additional (Fe^{m+}) site; this is explained in terms of electron delocalization, on the basis of a thermally activated electron exchange between Fe^{2+} and picolinium.

The assumption that the relative intensities reflect the iron populations (case of

identical f factors for Fe^{3+} and Fe^{2+}), which is the basis of our charge transfer model, is discussed, and the conditions for the validity of this assumption are determined in terms of "Mössbauer temperatures" $\theta_{M'}$ for the Fe^{3+} and Fe^{2+} sites.

The relatively high isomer shift near the room temperature (1.07 mm/sec at 210 K) and the high paramagnetic quadrupole splitting at low temperatures (2.60 mm/sec at 77 K) for the Fe^{2+} atoms, are indicative of "localized" $3d$ electrons, according to the δ and ΔE systematics for octahedral iron oxides. Nevertheless, despite this "localization," these iron atoms must be understood as resulting from a dynamic equilibrium in the Fe^{2+}–picolinium electron exchange, and as existing on the time scale of the Mössbauer effect, rather, than in the "infinite" time of any macroscopic measurement. The observed decreasing intensity of these atoms at higher temperatures and the appearance of Fe^{m+} sites confirm this point of view.

The Fe^{m+} atoms are believed to reflect a "delocalized" electronic state, different from a "mixture" of Fe^{3+} and Fe^{2+} ions. In this sense, the valence m is not an ionic charge state but a lumped electronic state, arising from electron delocalization, corresponding to an electronic density intermediate between those of Fe^{3+} and Fe^{2+}.

The apparent disagreement between the existence of electronic delocalization and the absence of any increase in the conductivity going from FeOCl to FeOCl(pic) seems to arise from an activation energy, which is related to the electron exchange process (from both the intensity $I(T)$ curve of the Fe^{m+} site and the application of the Lotgering and Van Diepen model) much lower than that deduced from the electrical resistivity $\rho(T)$ curve.

The fitted large linewidth suggests that the three iron sites of the paramagnetic region, i.e., Fe^{3+}, Fe^{2+}, Fe^{m+}, represent a more complex situation, of slightly inequivalent iron atoms in the vicinity of each site. This inequivalence causes the trapping of the electrons on inequivalent sites and is involved in the electron exchange process between inequivalent iron–picolinium pairs.

The spectra of the magnetic region, relative to those of FeOCl, seem to reflect both the existence of magnetically inequivalent iron sites and electronic relaxation and can be explained by different theories. From a comparison with other layered compounds, we have tentatively attributed the relaxation to the layers which, in light of the magnetic bidimensionality proposed from neutron diffraction studies for FeOCl, could exhibit superparamagnetic behavior, whose the mechanism is not explained.

The fitting of the spectra with a fixed angle θ for all sites shows that the magnetic properties are governed in large measure by crystalline anisotropy effects. These effects cause the hyperfine field (easy direction of magnetization) to lie in the layer plane in FeOCl(pic) and perpendicular to this plane in pure FeOCl. This result for pure FeOCl is consistent with the magnetic order proposed from neutron diffraction measurements.

The existing trends for δ, ΔE, H, and T_N values between FeOCl and the intercalated FeOCl$(G)_n$ compounds are not yet well understood. Any discussion requires detailed knowledge of the atomic electronic configurations, bonding, and magnetic interactions, and requires further work.

Appendix

There is, in our opinion, a confusion in the literature of FeOCl$(G)_n$ compounds concerning the signs of V_{zz} and the corresponding quadrupole interaction (ε_m) in the magnetic state (for the definition see Sect. 2.2.2). Kanamaru *et al.* (*28*) found a six-line spectrum ($\theta = 0$, $\eta = 0$) on FeOCl$(py)_{1/3}$ with $\varepsilon_m < 0$ ($|v_5 - v_6| < |v_1 - v_2|$) and

reported the same (negative) sign for the corresponding V_{zz}. This situation (same sign for ε_m and V_{zz}) is generally accepted in the Mössbauer literature (see, for example, Refs. (*53*, *75*)). Unlike this case, Herber *et al.* reported a difference in sign for V_{zz} as compared to ε_m. Therefore, they reported $V_{zz} > 0$ for $FeOCl(py)_{1/3}$ and $FeOCl(NH_3)_{3/4}$ with a negative ε_m (*19*, *20*), and $V_{zz} < 0$ for $FeOCl(TEP)_{1/6}$ (*20*), $FeOCl(TMP)_{1/6}$ (*20*), $FeOCl(pic)_{1/4}$ (*10*), and $FeOCl(butyl)_{1/4}$ (*19*) with a positive ε_m. With these explanations, the original statement of Herber and Maeda (*19*, *20*), $V_{zz} < 0$ for $n \leq 1/4$ and $V_{zz} > 0$ for $n \geq 1/3$, becomes, in terms of the ε_m formulation, $\varepsilon_m > 0$ for $n \leq 1/4$ and $\varepsilon_m < 0$ for $n \geq 1/3$. Retaining this last formulation, related to an experimental (and thus unambiguous) parameter of a "magnetic" spectrum, our result ($\varepsilon_m < 0$ for $n = 1/4$) is in disagreement with the rule Herber and Maeda. It is evident that, owing to the difference in V_{zz} and ε_m sign correlation between Kanamaru *et al.* and Herber *et al.*, the results obtained by these authors on $FeOCl(py)_{1/3}$ are in agreement concerning ε_m and in disagreement concerning V_{zz}.

References

1. S. KIKKAWA, F. KANAMARU, AND M. KOIZUMI, *Physica B* **105,** 249 (1981).
2. S. KIKKAWA, F. KANAMARU, AND M. KOIZUMI, *Bull. Chem. Soc. Japan* **52,** 96 (1979).
3. S. CLOUGH, P. PALVADEAU, J. P. VENIEN, *J. Phys. C.* **15,** 641 (1982).
4. J. ROUXEL AND P. PALVADEAU, *Rev. Chim. Miner.* **19,** 317 (1982).
5. P. PALVADEAU, J. P. VENIEN, to be published.
6. W. MENDENHALL AND R. L. SCHEAFFER, "Mathematical Statistics with Applications," p. 122 Duxbury, Belmont, Calif. (1973).
7. F. VARRET, A. GERARD, AND P. IMBERT, *Phys. Status Solidi B* **43,** 723 (1971).
8. P. PALVADEAU, L. COIC, J. ROUXEL, F. MENIL, AND L. FOURNES, *Mater. Res. Bull.* **16,** 1055 (1981).
9. N. N. GREENWOOD, F. MENIL, AND A. TRESSAUD, *J. Solid State Chem.* **5,** 402 (1972).
10. To our knowledge, the only evaluation of f values for the different Fe sites of a "multisite" compound is for the Fe_A and Fe_B sites in Fe_3O_4 (*11*) and other spinel ferrites (*12*).
11. G. A. SAWATZKY, F. VAN DER WOUDE, AND A. H. MORRISH, *Phys. Rev.* **183,** 383 (1969).
12. N. A. EISSA AND A. BAHGAT, *Phys. Status Solidi* **21,** 317 (1974).
13. F. K. LOTGERING AND A. M. VAN DIEPEN, *J. Phys. Chem. Solids* **38,** 565 (1977).
14. F. GRANDJEAN AND A. GERARD, *Solid State Commun.* **25,** 679 (1978).
15. R. H. HERBER AND R. A. CASSEL, *J. Chem. Phys.* **75**(9), 4669 (1981).
16. H. G. DRICKAMER, G. K. LEWIS, AND JR. S. C. FUNG, *Science* **163,** 885 (1969).
17. G. A. FATSEAS, J. L. DORMANN, AND H. BLANCHART, *J. Phys. (Paris)* **37,** C6-787 (1976).
18. C. D. SONG AND J. G. MULLEN, *Solid State Commun.* **17,** 549 (1975); *Phys. Rev. B* **14,** 2,761 (1976).
19. R. H. HERBER AND Y. MAEDA, *Inorg. Chem.* **20,** 1409 (1981).
20. R. H. HERBER AND Y. MAEDA, *Inorg. Chem.* **19,** 3411 (1980).
21. R. H. HERBER AND Y. MAEDA, *Physica B* **99,** 352 (1980).
22. K. MAHESH, *Phys. Status Solidi B* **61,** 695 (1974).
23. H. POLLAK AND W. BRUYNEEL, *J. Phys. (Paris)* **35,** C6-571 (1974).
24. J. B. GOODENOUGH AND G. A. FATSEAS, *J. Solid State Chem.* **41,** 1 (1982).
25. G. A. SAWATZKY AND F. VAN DER WOUDE, *J. Phys. (Paris)* **35,** C6-47 (1974).
26. R. W. GRANT, H. WIEDERSIGH, R. M. HOUSLEY, G. P. ESPINOSA, AND J. O. ARTMAN, *Phys. Rev. B* **3,** 678 (1971).
27. T. R. HALBERT, D. C. JOHNSTON, L. E. MC-.CANDLISH, A. H. THOMSON, J. C. SCANLON, AND J. A. DUMESIC, *Physica B* **99,** 128 (1980).
28. F. KANAMARU, M. SHIMADA, M. KOIZUMI, M. TAKANO, AND T. TAKADA, *J. Solid State Chem.* **7,** 297 (1973).
29. S. KIKKAWA, F. KANAMARU, AND M. KOIZUMI, *Inorg. Chem.* **19,** 259 (1980).
30. R. W. GRANT, *J. Appl. Phys.* **42,** 1619 (1971).
31. E. KOSTINER AND J. STEGER, *J. Solid State Chem.* **3,** 273 (1971).
32. T. ERICSSON AND R. WAPPLING, *J. Phys. (Paris)* **37,** C6-719 (1976).
33. D. L. NAGY, K. KULCSAR, G. RITTER, H. SPIERING, H. VOGEL, AND R. ZIMMERMANN, *J. Phys. Chem. Solids* **36,** 759 (1975).
34. F. VARRET AND P. IMBERT, *J. Phys. Chem. Solids* **5,** 215 (1974).

35. C. BOEKEMA, F. VAN DER WOUDE, AND G. A. SAWATZKY, *J. Phys. (Paris)* **37,** C6-603 (1976).
36. G. A. FATSEAS AND J. B. GOODENOUGH, *J. Solid State Chem.* **33,** 219 (1980).
37. H. SCHAFER-STAHL AND R. ABELE, *Z. Anorg. Allg. Chem.* **465,** 147 (1980).
38. W. M. REIFF, *in* "Mössbauer Effect Methodology" (I. J. Gruverman, Ed.), Vol. 8, p. 89, Plenum, New York (1973).
39. J. M. DANIELS AND A. ROSENCWAIG, *J. Phys. Chem. Solids* **30,** 1561 (1969).
40. See, for example, Ref. (*41*) and a recent review paper, Ref. (*42*).
41. V. BUCHENAU, *Phys. Status Solidi B* **70,** 181 (1975).
42. J. M. HONIG, *J. Solid State Chem.* **45,** 1 (1982).
43. J. M. COEY, A. H. MORRISH, AND G. A. SAWATZKY, *J. Phys. (Paris)* **32,** C1-271 (1971).
44. B. J. EVANS AND H. NAM OK, *Physica B* 86-88, 931 (1977).
45. R. PARKER AND C. J. TINSLEY, *Phys. Status Solidi A* **33,** 189 (1976).
46. J. B. GOODENOUGH, *Prog. Solid State Chem.* **5,** 509 (1971).
47. A. A. BAHGAT, M. K. FAYEK, A. A. HAMALAWAY, AND N. A. EISSA, *J. Phys. C* **13,** 2601 (1980).
48. H. SCHAFER-STAHL AND R. ABELE, *Angew. Chem. Int. Engl. Ed.* **19,** 477 (1980).
49. G. VILLENEUVE, P. DORDOR, P. PALVADEAU, AND J. P. VENIEN, *Mater. Res. Bull.* **17,** 1407 (1982).
50. A. ADAM AND G. BUISSON, *Phys. Status Solidi* **30,** 323 (1975).
51. J. DEZSI AND M. FODOR, *Phys. Status Solidi* **15,** 247 (1966).
52. C. E. JOHNSON, *J. Phys. C* **2,** 1996 (1969).
53. F. VAN DER WOUDE AND A. J. DEKKER, thesis; F. VAN DER WOUDE RIJKSUNIVERSITEIT TE GRONINGEN, (Ed.), "Brondez-Offset," Rotterdam (1966).
54. S. MORUP, "Paramagnetic and Superparamagnetic Relaxation Phenomena Studied by Mössbauer Spectroscopy, thesis, Polytecknisk Forlag 1981, Laboratory of Applied Physics II, Technical University of Denmark, Lyngby, Denmark.
55. J. LAVER, W. KEVNE, AND T. SHINKO, *Physica B* **86–88** 1409 (1977).
56. D. W. COLLINS, J. T. DEHN, AND J. N. MULAY, in "Mössbauer Effect Methodology" (I. J. Gruverman, Ed.), Vol. 3, p. 103, Plenum, New York (1967).
57. A. M. VAN DER KRAAN, *Phys. Status Solidi A* **18,** 215 (1973).
58. M. EIBSCHUTZ AND S. SHTRIKMAN, *J. Appl. Phys.* **39,** 997 (1968).
59. The hyperfine field is much more sensitive to covalency than the isomer shift (see, for example, Ref. (*24*)).
60. M. M. N. GUYEN-TRUT-DINH, M. VLASSE, M. PERRIN, AND G. LE FLEM, *J. Solid State Chem.* **32,** 1 (1980).
61. G. P. GUPTA, D. P. E. DICKSON, AND G. E. JOHNSON, *J. Phys. C.* **13,** 2071 (1980).
62. L. M. LEVINSON, M. LUBAN, AND S. SHTRIKMAN, *Phys. Rev.* **177,** 864 (1969).
63. F. VAN DER WOUDE, C. BLAAUW, AND A. J. DEKKER, Proceedings, International Conference on Mössbauer Spectroscopy Tihany, June 1969 (I. Dezsi, Ed.), p. 133. Academiai Kiado, Budapest (1971).
64. G. K. WERTHEIM, D. N. E. BUCHANAN, AND H. J. GUGGENHEIM, *Phys. Rev.* **152,** 527 (1966).
65. V. PETROULEAS, A. SIMOPOULOS, AND A. KOSTIKAS, *Phys. Rev. B* **12,** 4675 (1975).
66. H. KESSLER AND SON LY, *J. Solid State Chem.* **39,** 22 (1981).
67. J. L. FOURQUET, R. DE PAPE, J. TEILLET, F. VARRET, AND G. C. PAPAEFTHYMIOU, *J. Magn. Magn. Mater.* **27,** 209 (1982).
68. J. PIEKOSZEWSKI AND J. SUWALSKI, Proceedings, International Conference on Mössbauer Spectroscopy, Tihany, June 1969 (I. Dezsi, Ed.), p. 499, Academiai Kiado, Budapest (1971).
69. E. KNELLER, M. VELICESCU, AND F. HABEREY, *J. Magn. Magn. Mater.* **7,** 49 (1978).
70. S. C. BARGAVA, S. MORUP, AND J. E. KNUDSEN, *J. Phys. (Paris)* **37,** C6-93 (1976).
71. E. DE GRAVE, R. VAN LEERBERGHE, C. DAUME, J. DESITTER, AND A. GOVAERT, *J. Phys. (Paris)* **37,** C6-97 (1976).
72. H. TH. LE FEVER, F. J. VAN STEENWIJK, AND R. C. THIEL, *Phys. B* **86–88,** 1269 (1977).
73. A. ITO AND M. HORIJKE, *J. Phys. (Paris)* **40,** C2-323, C2-290 (1979).
74. H. KELLER, W. KUNDIG, AND H. AREND, *Physica B* **86–88,** 683 (1977).
75. J. M. D. COEY AND G. A. SAWATZKY, *Phys. Status Solidi B* **44,** 673 (1971).